MDCT of the Airways: Technique and Normal Results

Catherine Beigelman-Aubry, MD[a], Pierre-Yves Brillet, MD, PhD[b], Philippe A. Grenier, MD[a,*]

KEYWORDS

- Trachea anatomy • Bronchi anatomy
- Airway dimensions • Airway MDCT technique

Previously, the trachea and main bronchi were assessed with a variable slice thickness up to 5 mm with sequential or volumetric CT, and small airways diseases were explored with high-resolution CT (HRCT), based on a 1.5-mm slice at 10-mm intervals. Currently, the new generation of multidetector CT (MDCT) by combining volumetric CT acquisition and thin collimation during a single breathhold provides an accurate continuous assessment from the trachea to the most distal airway visible. Isotropic voxels allow image reconstructions in which the z dimension is equivalent to the x and y (in plane) resolution.[1] This approach creates multiplanar reformations of high quality along the long axis of the airways[2] and three-dimensional volume rendering, including extraction of the airway and virtual endoscopy without any distortion in any orientation. Whatever their nature and severity, excellent assessments of stenoses may be obtained by a combination of various reconstructions, especially the determination of the morphology, including the identification of horizontal webs and the length and exact location from the vocal cords and carina.[3,4] Airway stents and extrinsic airway compression are also assessed perfectly. Preprocedural planning before stent placement or surgery[3] and posttherapeutic aspects also benefit from the same techniques. Despite images usually being obtained during suspended inspiration for analysis of airways, a complementary acquisition during forced expiratory maneuver may be requested to assess the degree of tracheobronchomalacia and the extent of air trapping.

IMAGE ACQUISITION AND RECONSTRUCTION

Because the lung parenchyma offers a unique natural contrast, low radiation dose may be used without significant loss of information (100–120 kV, 60–160 mAs). Using a detector size of 0.625 mm with MDCT, images are reconstructed with a slice thickness of approximately 1 mm and overlapped with a reconstruction interval of approximately one-half slice thickness. This produces a resolution voxel of almost cubic dimensions of approximately 0.4 mm in each direction by using a spatial resolution algorithm. Experts recommend using a 512 or even a 768 matrix, which permits fields of view of 265 mm and 400 mm, respectively. The pixel size at the workstation, which is defined as the ratio between the field of view and the matrix, has to be lower than the intrinsic resolution in the plane of image to benefit from the intrinsic resolution capabilities of the equipment.[5]

A rotation time of approximately 500 msec allows an important decrease in cardiac pulsation artifacts and allows a good analysis of all bronchi, including the paracardiac areas. Breathholding for acquisition of the entire chest lasts approximately 6 to 8 seconds using a 40 or 64 detector row CT scanner, which avoids respiratory motion artifacts

[a] Service de Radiologie, Hôpital Pitié-Salpêtrière, Assistance Publique-Hôpitaux de Paris (APHP), Université Pierre et Marie Curie, 47/83 boulevard de l'Hôpital, 75651 Paris cedex 13, France
[b] Service de Radiologie, Hôpital Avicenne, Assistance Publique-Hôpitaux de Paris (APHP), Université Paris XIII, UPRES EA 2363, Hôpital Avicenne, 125, route de Stalingrad, 93009 Bobigny, France
* Corresponding author.
E-mail address: philippe.grenier@psl.aphp.fr (P.A. Grenier).

Radiol Clin N Am 47 (2009) 185–201
doi:10.1016/j.rcl.2009.01.001

in most cases. The use of cardiac gating is not recommended because of the higher radiation dose delivered and short rotation time available with the last generations of MDCT.

READING AND POSTPROCESSING TOOLS

Cine Viewing

Visualization of overlapped thin axial images sequentially in a cine mode allows analysis of bronchial divisions from the segmental origin down to the smallest bronchi that can be identified on thin section images. Particular attention must be paid to the analysis of the lumen of the tracheobronchial tree, the airway walls, and the spurs at the same time. Moving up and down through the volume at the monitor has become a useful alternative to film-based review. This viewing technique helps indicate the exact location of any airway lesion and may serve as a roadmap for the endoscopist. Reading of chest MDCT goes actually far beyond the standard assessment of axial slices, because multiplanar reformats are easily performed in real time in all directions[6] and slabs with various rendering modes. Once any abnormality has been detected, an oblique reformat plane may be chosen with the swivel mode by focusing a rotation center on the abnormality

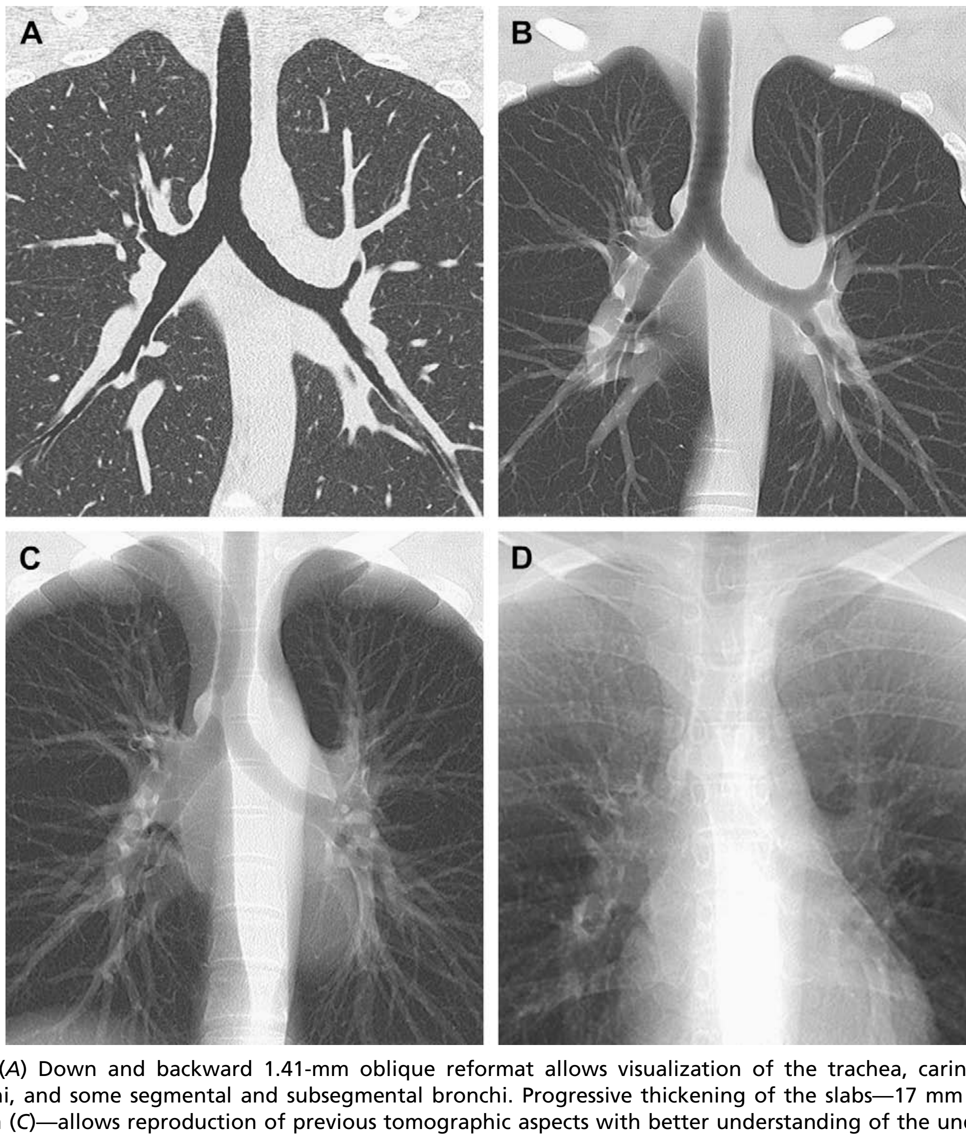

Fig. 1. (*A*) Down and backward 1.41-mm oblique reformat allows visualization of the trachea, carina, main bronchi, and some segmental and subsegmental bronchi. Progressive thickening of the slabs—17 mm (*B*) and 54 mm (*C*)—allows reproduction of previous tomographic aspects with better understanding of the underlying pathology, especially for the airways. (*D*) Slab average of 180 mm thickness allows reproduction of the aspect of the frontal chest radiograph. The right tracheal stripe is clearly explained by the correlation on (*A*).

found. A combination of slabs of various thicknesses with minimum intensity projection (mIP) or maximum intensity projection (MIP) or both usually is obtained.

Two-Dimensional Reformats and Multiplanar Volume Rendering Slabs

Reformations and reconstructions are easy to generate and may be interactively performed in real-time at the console or workstation. Multiplanar reformation images are single-voxel sections with a 0.6- to 0.8-mm displayed image. They are the easiest reconstructions to generate and permit creation of images oriented in any plane, especially along the long axis of any airway (eg, in a coronal oblique orientation for the trachea and the carina). On the other hand, multiplanar volume reformation consists of a slab of adjacent thin slices of various thicknesses that may be combined with the use of intensity projection techniques. The reformation plane may be selected by focusing a rotation center on the abnormality and using the swivel mode or using a three-dimensional reconstructed image of the airways.[7] A significant decrease in the number of slices to be analyzed is achieved by analysis of longitudinal reformats compared with the axial images with a complementary role of both viewing techniques.

Analysis of various large and small airway diseases may be enhanced with this technique. In fact, multiplanar volume reformation images combine the excellent spatial resolution of multiplanar reformats images with the anatomic display of thick slices[8] and the possibility of using various rendering tools:

- Average: the mean attenuation value of the voxels in every view throughout the volume explored is projected on a two-dimensional image. A less noisy image may be obtained de facto. Tomographic equivalent images may be obtained by thickening the slabs with equivalent of plain films in the coronal and lateral views with the thickest slabs (**Fig. 1**).
- mIP imaging is a simple form of volume rendering (sliding thin slab or multiplanar volume reformation mIP technique) that is able to project the tracheobronchial air column onto a viewing plane by projecting the pixels with the lowest attenuation value. This technique enhances the visibility of the airways within lung parenchyma below the subsubsegmental level because of lower attenuation of air contained within the tracheobronchial tree compared with the surrounding pulmonary parenchyma (**Fig. 2**), with a difference of density between 50 and 150 HU.[9] The overall morphology of the tracheobronchial tree is particularly well displayed on longitudinal views combined with a multiplanar volume reformation mIP technique. Three- to 7-mm slabs are particularly adapted for the assessment of central airways stenosis, but the slab thickness may be chosen according to the complexity and morphology of the abnormality and may be increased up to several centimeters. Abnormal lucencies, including bronchial wall diverticula observed in patients who have chronic obstructive pulmonary disease and bronchial anastomosis, dehiscence, or fistula during or after lung transplantation, may be assessed using the same technique. Multiplanar volume reformation mIP is also used for a systematic analysis of the parietal wall and lumen of the bronchi. This analysis also includes the assessment of peribronchial thickening encountered in case of lung diseases with a perilymphatic distribution. In chronic bronchial disease, bronchial wall thickening is often irregular and associated with thickening of the spurs and irregularities in the morphology and caliber of the bronchi. This technique may help plan the correct bronchoscopic pathway toward a distal lesion for biopsy. Postexpiratory mIP

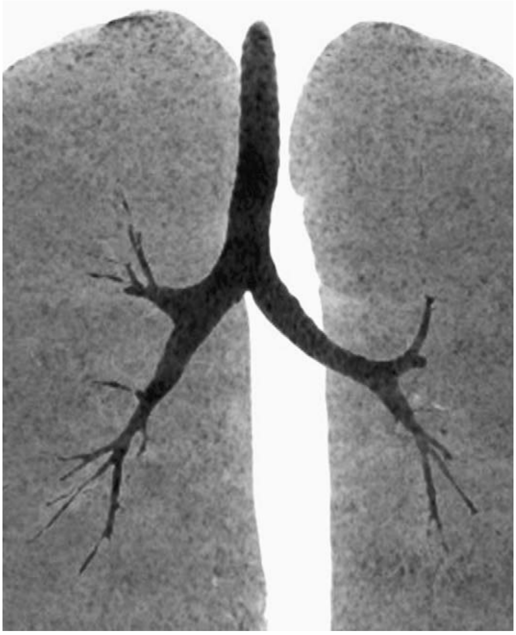

Fig. 2. Coronal mIP 60-mm slab allows display of the normal bronchial tree to the subsegmental level.

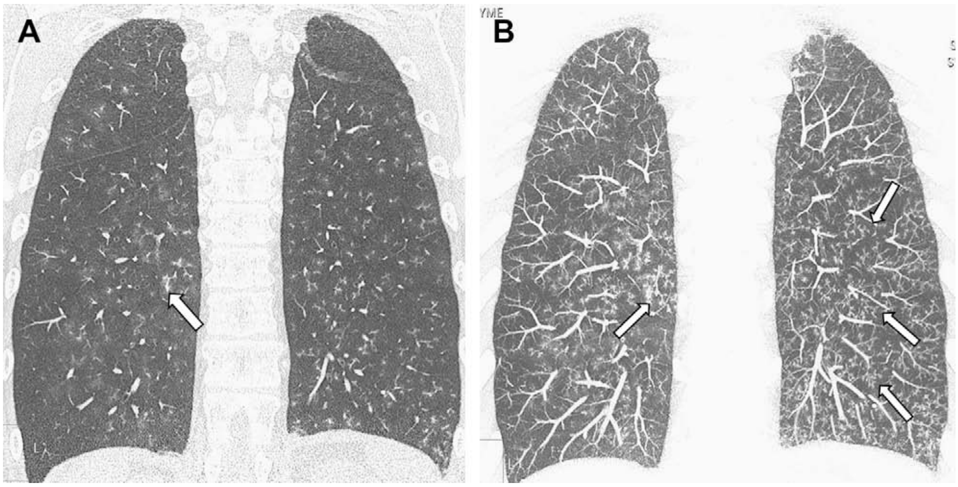

Fig. 3. Single (*A*) and 14-mm slab MIP (*B*) coronal reformats in a patient suffering from infectious bronchiolitis. (*A*) Patchy ground-glass bronchoalveolar nodules with bronchial wall thickening (*white arrow*). (*B*) Diffuse tree in bud aspects (*black and white arrows*) difficult to assess in (*A*) are obvious with MIP.

images may be useful for detecting and assessing the extent of air trapping.

- MIP consists of projecting the voxel with the highest attenuation value in every view through the volume explored.[10,11] It displays 10% of the data set, as does the mIP technique. Centrilobular nodules related to inflammatory or infectious changes in the small airways are easily recognized with respect to landmarks of the secondary pulmonary lobule (**Fig. 3**).[12] A rapid assessment of the regional distribution in the craniocaudal and axial dimensions is obtained at the same time. MIP of variable thickness also provides an excellent assessment of the location and size of vessels. In this way, mosaic perfusion pattern is diagnosed by combination of mIP and MIP and is easily differentiated from mosaic attenuation pattern caused by infiltrative lung disease.

External Three-Dimensional Rendering Technique

The volume-rendering technique applied at the level of the airways ensures a three-dimensional reconstruction of the airways to the subsegmental level by depicting the inner surface of the airway with a specific color and opacity (**Fig. 4**). It has capabilities of visualization in semi-transparent mode similar to conventional bronchograms.[13] For this reason, this technique has been referred as CT bronchography. Three-dimensional segmentation techniques provide an anatomic map of the airways and easily may demonstrate changes between inspiration and expiration in the case of tracheomalacia.

This technique has proved to be of particular interest in diagnosing mild changes in airway caliber and understanding complex tracheobronchial abnormalities.[14] When correlating bronchoscopy and three-dimensional reconstructions, Kauczor and colleagues[15] observed no

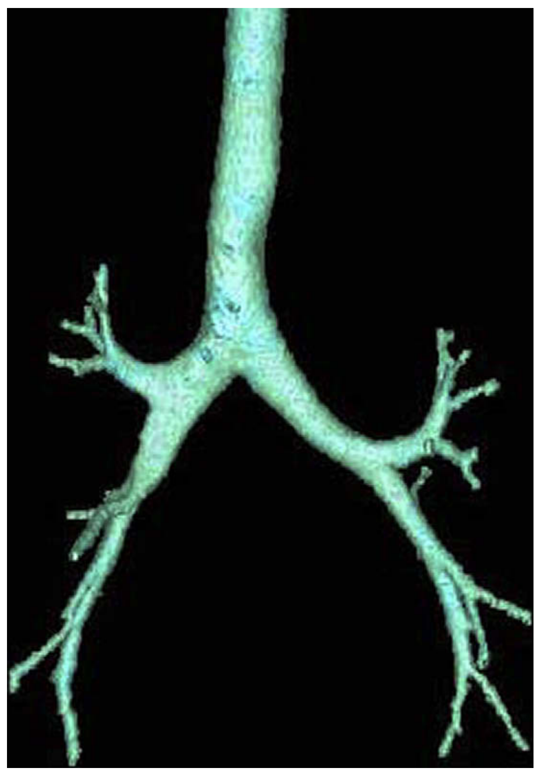

Fig. 4. Three-dimensional volume rendering of a normal tracheobronchial tree.

discrepancies concerning the location and severity of central stenoses. Three-dimensional helical CT provided an accurate road map for the central airways. Clinical relevance in patients with tumors resulted from severe stenoses or occlusions that lead to dyspnea and stridor. When bronchoscopy revealed severe stenosis or total occlusion, the patency of distal bronchi, tumor involvement, or collapse could not be assessed bronchoscopically. In comparison, three-dimensional helical CT was superior at showing the residual lumen and length of the stenoses, spatial orientation, branching angles, and patency of distal air-filled bronchi. These complementary details were important for possible endobronchial procedures such as laser ablation, stent placement, and transbronchial radiotherapy. This approach facilitated the choice of endobronchial procedures, and the size of the stent could be determined accurately.

Using the same concept, Fetita and colleagues[16] developed a fully automatic method for three-dimensional reconstruction of the tracheobronchial tree based on bronchial lumen detection within the thoracic volume data set obtained from thin MDCT acquisition. It provides a specific visualization modality that relies on energy-based three-dimensional reconstruction of the bronchial tree up to the sixth or seventh order subdivisions with a semi-transparent volume rendering technique.[17] Automatic delimitation and indexation of anatomic segments make local and reproducible analysis possible at any level of the bronchial tree. Automatic extraction of the central axis of the bronchial tree allows interactivity during navigation within CT bronchography or virtual endoscopy modes.

Internal Rendering Technique or Virtual Bronchoscopy

Virtual bronchoscopy by combining helical CT data and virtual reality computing techniques[13]

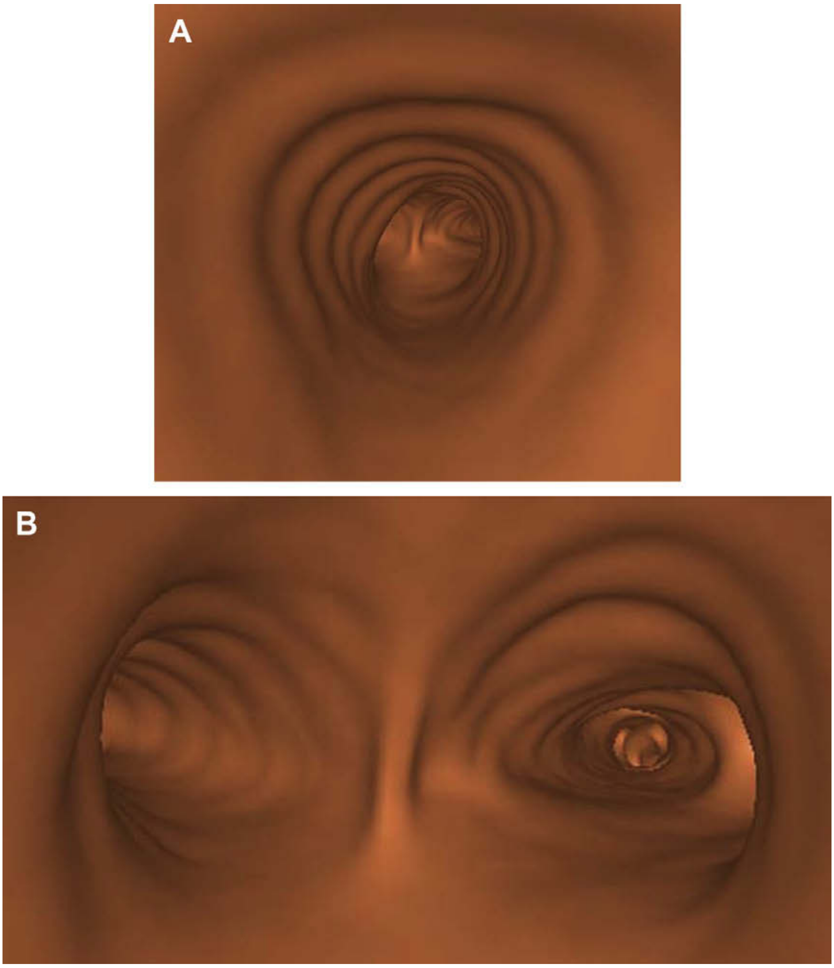

Fig. 5. Virtual endoscopy at the level of the middle trachea (*A*) and the carina (*B*).

provides an internal rendering of the tracheobronchial walls and lumen by using reconstruction with soft kernel. An endoscopist's view of the internal surface of the airways is simulated with a perspective-rendering algorithm (**Fig. 5**). The observer may interactively move through the airway at a rate of 15 to 25 images/second down to the subsegmental bronchi. Potential applications include the assessment of airway stenoses and guidance of transbronchial biopsy procedures.[18] The technique allows accurate reproduction of major endoluminal abnormalities and has excellent correlation with fiberoptic bronchoscopy results regarding the location, shape, and severity of airway narrowing. Virtual bronchoscopy is also able to evaluate the airways distal to a high-grade stenosis, beyond which a conventional bronchoscope cannot pass.[19] It is also possible to perform retroscopy when looking back toward the distal part of the stenosis. Virtual endoscopy may be considered a substitute for repeated bronchoscopies when performed in the follow-up of interventional procedures.[20] Despite its potential, virtual endoscopy is unable to identify the causes of bronchial obstruction[21] or detect mild stenosis, submucosal infiltration, and superficial spreading tumors.[4]

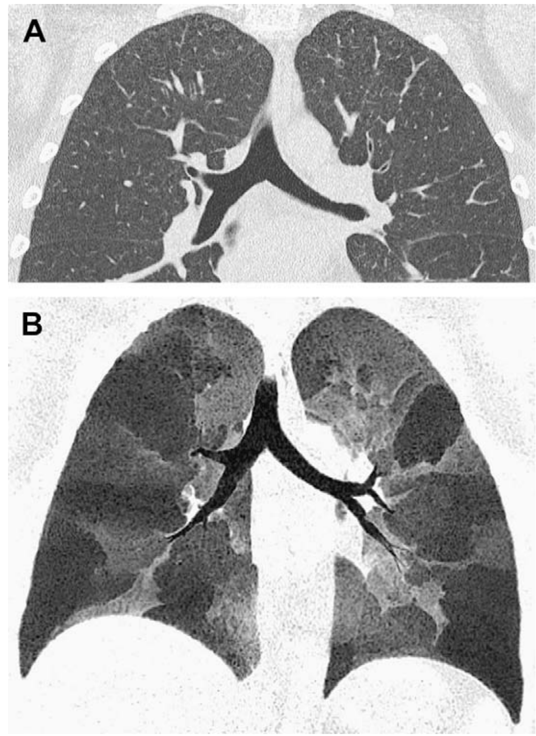

Fig. 6. Patient suffering relapsing polychondritis. (*A*) Normal aspect on inspiration is visualized on a volume from the vocal cords to the lower pulmonary veins. (*B*) Multifocal air trapping is assessed on 20-mm slab coronal mIP reformat despite the fact that the acquisition was performed with only 15 mAs.

LEVEL OF BREATHING

All CT examinations of the airways are first performed at suspended full inspiration. In case of suspicion of mosaic attenuation or bronchomalacia, expiration has to be performed on a dynamic mode. In fact, this technique has proved to optimize the detection of air trapping, which is an indirect sign of small airway disease,[22] and tracheobronchomalacia.[23] The advantage of volumetric acquisition in this setting is use of mIP that enhances the visual detectability of air trapping and may increase the conspicuity of this finding,[24] even using low-dose CT (**Fig. 6**).[25]

QUANTITATIVE CT ASSESSMENT OF AIRWAYS

Airway lumen and airway wall areas may be assessed quantitatively on CT images by using specific techniques that must be reproducible and accurate to compare the airways before and after therapy and carry out longitudinal studies of airway remodeling. Because airway lumen and wall areas measured on axial images depend on lung volume, volumetric acquisition at controlled lung volume is required to precisely match the airways of an individual on repeated studies. Lumen and wall areas measured on axial images also depend on the angle between the airway central axis and the plane of section. Measuring airway lumen and airway walls when they are not perpendicular to the scanning plane may lead to significant errors related to an overestimation of airway wall area, as in the case of oblique bronchi. The larger the angle and field of view and the thicker the collimation, the greater the overestimation of airway wall area. Accurate measurements of airway lumen and wall area have to be restricted to airways that appear rounded (ie, cut in cross-section). The new generation of multislice CT scanner allows segmentation of bronchial lumens with three-dimensional reconstruction of the airways, extraction of the central axis of the airways, and reconstruction of the airway cross-section in a plane perpendicular to this axis (**Fig. 7**).[26]

Numerous techniques have been reported for measuring airway diameter using CT. They have been validated using data from phantom studies and excised animal lungs or by developing realistic modeling of airways and pulmonary arteries included in CT scans of animal lungs obtained in vivo.[27–32] These techniques have proved to be more accurate than those obtained with manual

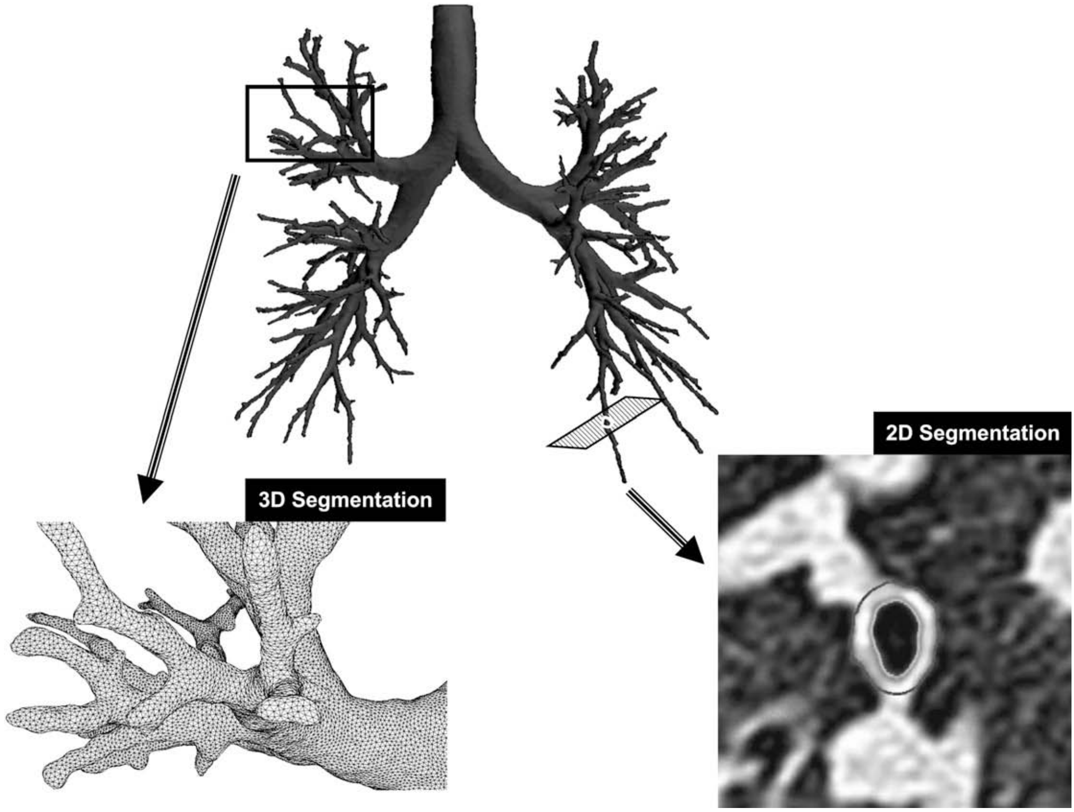

Fig. 7. Segmentation of bronchial lumens with three-dimensional reconstruction of the airways, extraction of the central axis of the airways, and reconstruction of a subsegmental branch of the posterior basal segmental bronchus of the left lower lobe (LLL) cross-section in a plane perpendicular to this axis.

methods. In fact, manual tracing of the inner and outer contours of the airway cross-section on axial CT images is a time-consuming technique that suffers from large intra- and interobserver variability in measurement of airway wall and lumen areas.[29,33–35] Their accuracy in measuring the airway lumen[27–29,31] and wall[28,30] areas was good only for bronchi that measured at least 2 mm in diameter. These techniques have been used to quantify the magnitude and distribution of airway narrowing in excised lung animals and animal lungs in vivo and in normal patients and patients who have asthma.[27,29,36–38] Although the techniques have been used almost exclusively for research purposes, with continued refinements they eventually will be beneficial in the clinical practice of radiology.[39–41]

NORMAL ANATOMY AND NORMAL CT FINDINGS

Trachea

The conducting airways that distribute air to the gas-exchanging units begin with the trachea. The trachea, which originates at the inferior margin of the cricoid cartilage at the level of the sixth cervical vertebra to the carina at the level of the fifth thoracic vertebra, has an oblique course downwards and backwards. Its length on inspiration has a value of 10 to 12 cm in adults, including the extrathoracic (2–4 cm) and intrathoracic portions (6–9 cm).[42,43] Changes in position may be observed between inspiration and expiration,[44] up to 3 cm, and with neck flexion and extension.

Adjacent structures directly related to the trachea are the thyroid gland, which is anterior and lateral to the cervical trachea, vessels anterior to the intrathoracic trachea (supra-aortic vessels, aortic arch, pulmonary arteries), systemic veins (superior vena cava, azygos vein), which are anterolateral or lateral to the trachea, lymph nodes, the esophagus, which is posterior or lateral to the trachea, and the left recurrent nerve. The trachea is often displaced slightly to the right at the level of the aortic arch, which may be accentuated in older patients with tortuous atherosclerotic aorta. The right or posterior tracheal wall contacts the right lung at a variable extent.[42]

The tracheal wall is comprised of several layers, including an inner mucosa layer, a submucosa, cartilage or muscle, and an outer adventicia layer. The anterior walls of the trachea and main bronchi are formed with U-shaped rings of hyaline cartilage—16 to 22 for the trachea—that open dorsally. These rings are linked longitudinally by annular ligaments of fibrous and connective tissue and help support the tracheal wall and maintain an adequate tracheal lumen during forced expiration.[43] The flat dorsal wall consists of a thin fibromuscular membrane that includes the trachealis muscle, which is composed by transversely disposed smooth muscle.[45]

The cross-sectional appearance of the trachea is most commonly rounded, oval, or horseshoe shape on inspiration, with a posterior wall that is typically flat or convex posteriorly. Several shapes may be encountered at different levels.[42] The right wall of the inferior aspect of the trachea is in contact with air within the medial aspect of the right upper lobe, which results in the right paratracheal stripe seen in routine posteroanterior chest radiographs with a normal size less than 4 mm. The tracheal wall appears as a 1- to 3-mm soft-tissue stripe between the air-filled tracheal lumen and the lateral fat density of the mediastinum.[42,46,47] Normal cartilaginous rings may appear slightly denser than surrounding soft tissue and fat. Calcification of the cartilage is commonly seen in older patients, particularly women, at the level of the trachea and more distal bronchi (**Fig. 8**). These calcifications are usually discontinuous.[42]

The normal transverse diameter of the trachea in men and women is 13 to 25 mm and 10 to 21 mm, respectively, and the normal anteroposterior diameter in men and women is 13 to 27 mm and 10 to 23 mm, respectively. The tracheal diameter averages 19.5 mm in men and 17.5 mm in women.[43,46,48] A mean decrease in the transverse diameter of approximately 15%, in the anteroposterior diameter of approximately 30%, and in the cross-sectional area of the trachea of approximately 35% is observed on forced expiration, mainly related to invagination of the posterior tracheal membrane. On expiration, the posterior tracheal membrane appears convex anteriorly; the horseshoe shape ensures actual patient expiration. Tracheomegaly is defined in men as a tracheal diameter of more than 25 mm in the transverse diameter and more than 27 mm in the anteroposterior dimension. In women it is defined as tracheal diameter of more than 21 mm in the transverse diameter and more than 23 mm in the anteroposterior dimension.[49]

The tracheal index is obtained by dividing the coronal diameter by the sagittal one, with a normal value of approximately 1.[42,43,47] A "saber sheath trachea" is characterized by a marked coronal narrowing with a tracheal index of less than 0.5. This finding is suggestive of chronic obstructive lung disease with emphysema. Conversely, a "lunate" configuration with a ratio of more than 1 suggests tracheomalacia related to excessive expiratory collapsibility of the airway lumen.[50]

Main, Lobar, Segmental, Subsegmental Bronchi and Small Airways

The trachea gives rise to the right and left main bronchi with an asymmetrical branching. The left main bronchus is narrower than the right one, with a length of approximately 5 cm[51] and a typical elliptical shape and branches off at a greater angle than the right.[52] The left main bronchus branches into the left upper and lower lobe bronchi. The right bronchus is shorter than the left one and extends for 1 to 2 cm before dividing into the right upper lobe bronchus and the bronchus intermedius. Within the lung, the bronchi branch dichotomously and give rise to progressively smaller airways. Branching is asymmetrical, taking into account that the two daughters of a given branching may differ in diameter, length, and angle. The number of generations from the main bronchus to the acini varies from as few as 8 to as many as 25, depending on the region of the lung supplied.[52] The lobar bronchi branch off to segmental bronchi.

Several systems for labeling segmental anatomy have been proposed, mainly the Jackson and Huber and the Boyden classifications.[53,54] Segmental bronchi are designated by "B" followed by a number, and subsegmental bronchi are indicated by the segmental number followed by a lower case letter. The numbering of the segmental bronchi corresponds to their order of origin from the airway. Although the segmental bronchial anatomy varies, the right lung contains ten segmental bronchi and the left contains eight in most patients. The first Boyden classification, which initially designated the anterior segment as B2 and the posterior segment as B3, is used in this article (**Figs. 9–12**). Identification of the origin of most bronchi depends on recognizing the spurs that separate them. Depending on its angle relative to the CT plane, a spur appears either as a triangular wedge of soft tissue or, when sectioned along its length, as a linear septum that separates adjacent airways or faint curvilinear densities.[45]

After branching off the pulmonary artery below the aortic arch, the right pulmonary artery enters the lung anterior to the right main bronchus; the left pulmonary artery passes above the main

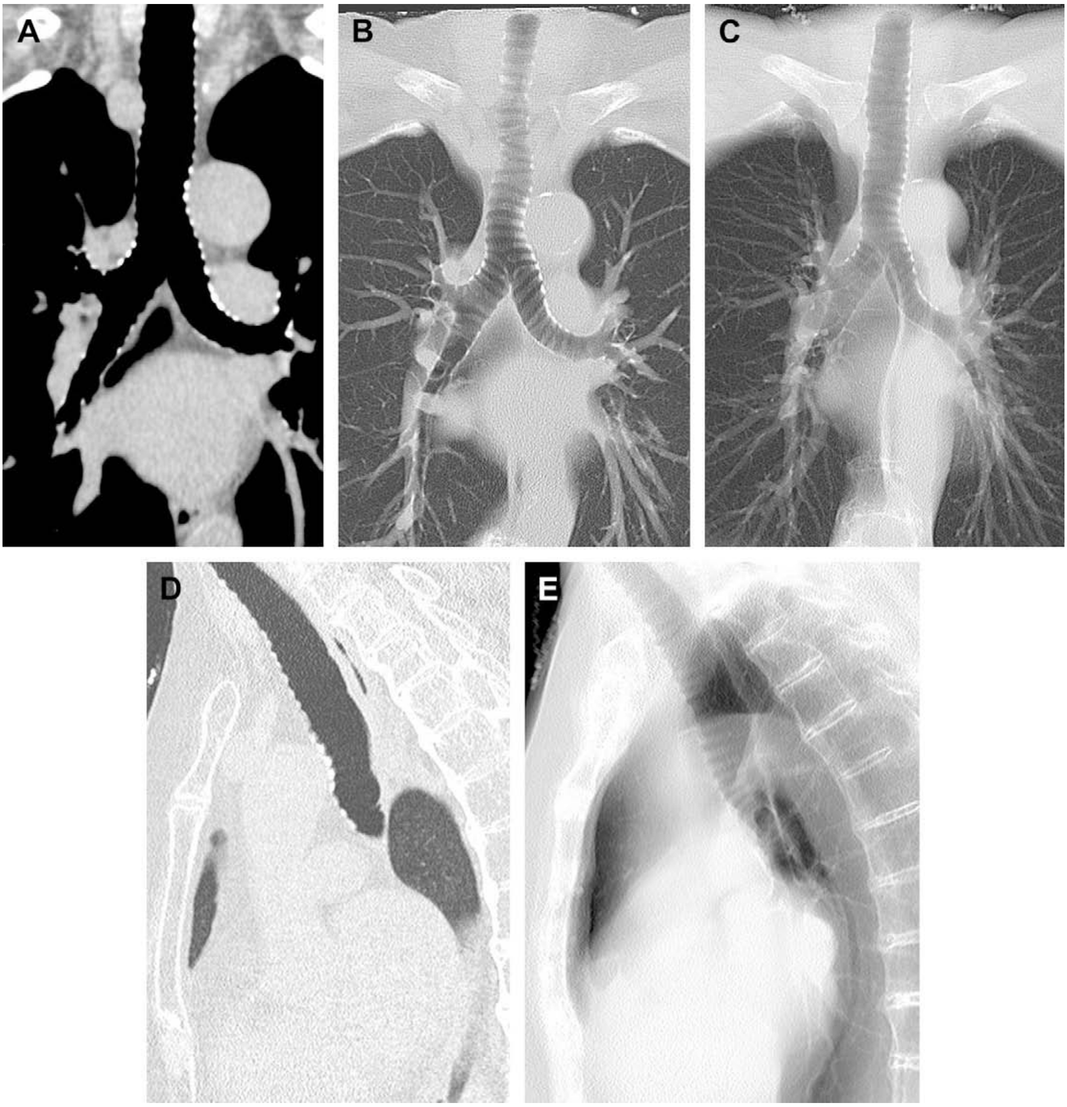

Fig. 8. Single (*A*), 3-mm (*B*), and 11-mm (*C*) slabs average coronal reformats perfectly demonstrate the calcified tracheal rings in a normal older woman. Single (*D*) and 62-mm (*E*) slab average sagittal reformats. The lack of cartilage at the level of the posterior wall of the trachea is well seen (*arrows*). Conversely, the ring cartilages that are partially calcified are obvious at the level of the anterior and lateral part of the trachea (*arrows*).

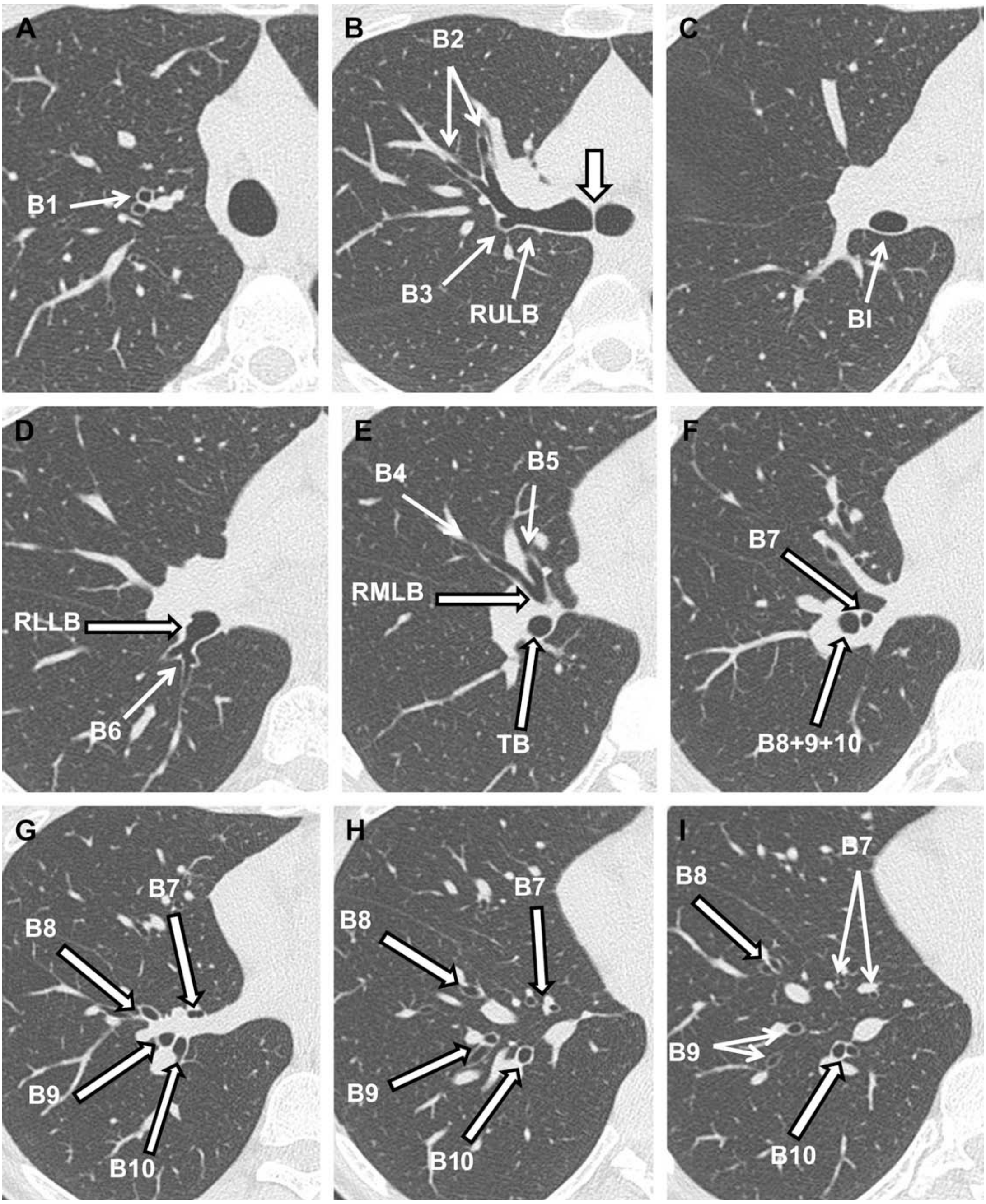

Fig. 9. Normal anatomy of the bronchi on the right side. The first Boyden's classification is used with successive 1-mm slices. (*A*) The arrow shows the division of the apical bronchus of the right upper lobe. Note the oval shape of the normal trachea. (*B*) Right upper lobe bronchus arises from the lateral aspect of the main bronchus, approximately 2 cm distal to the carina (*large arrow*) and courses horizontally for approximately 1 cm from its origin before dividing in segmental branches. Subsegmental bronchi of the anterior bronchus of the right upper lobe are marked by arrows. (*C*) The bronchus intermedius divides after 3 to 4 cm into the middle lobe and lower lobe bronchi. (*D–F*) The middle lobe bronchus arises from the anterolateral wall of the bronchus intermedius and courses anteriorly and laterally for 1 to 2 cm before dividing into lateral (B4) and medial (B5) branches. This origin of the middle lobe is almost at the same level as B6, which is the first branch of the short right lower lobar bronchus (RLLB). The superior segmental bronchus B6 and its subsegmental bronchi arise from the posterior aspect of the RLLB just beyond its origin and course posteriorly. The truncus basalis represents a continuation of the lower lobar bronchus below the origin of B6 and typically appears circular or ovoid. It extends for approximately 1 cm before dividing in four basal segmental bronchi. The first basal bronchi is the medial basilar segmental bronchus (B7) that arises anteromedially from the TB. (*G–I*) Next, there is a successive appearance of the anterior, lateral (B9), and posterior basilar (B10) bronchi and their respective subsegmental bronchi. Note that B7 and its subsegmental bronchus lie typically anterior to the inferior pulmonary vein. (*J*) 3D volume rendering.

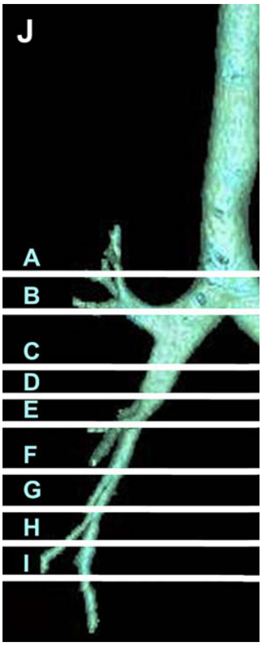

Fig. 9. (*continued*).

stem bronchus and then over the superior lobar bronchus, coming to lie posterior to the bronchus. Within the lung parenchyma, the bronchi and pulmonary artery branches are closely associated and branch in parallel until they reach the acini. Their appearance depends on their orientation. When imaged at an angle to their longitudinal axis, central pulmonary arteries normally appear as rounded or elliptic opacities accompanied by uniformly thin-walled bronchi of similar size and shape. Bronchi and pulmonary arteries appear as cylindrical structures that taper as they branch when imaged along their long axes; they appear rounded if they lie perpendicular to the plane of the CT or elliptical when oriented obliquely. Bronchi and arteries are encased by the peribronchovascular interstitium, which extends from the pulmonary hila into the peripheral lung. The pulmonary veins drain independently from the bronchi with two trunks that enter the left atrium separately.

All conducting airways are muscular tubes lined by a ciliated epithelium. Bronchi with a diameter of approximately 1 mm or more have walls reinforced by cartilage, which take the form of variably shaped islands that diminish in size and number progressively with the decreasing caliber of the bronchi. According to Hayward and Reid,[55] a high density of cartilage was observed for the first four to six generations that effectively provided a circumferential support; the axial bronchi had only scattered plates for another four to six generations. Bronchioles are conducting airways with a wall less than 1 mm in diameter consisting in smooth muscle enclosed in a thin connective tissue space without cartilage. Membranous bronchioles do not contain alveoli, as opposed to respiratory bronchioles, which are lined partly by alveoli. The terminal bronchioles identify the most distal generation of membranous bronchioles, that is, the parent generation to the respiratory bronchioles. Two to three additional generations of respiratory bronchioles are present after the most proximal branch.

The outer diameter of a bronchus is approximately equal to that of the adjacent pulmonary artery. The normal bronchoarterial ratio, defined as the internal diameter (ie, luminal diameter) of the bronchus divided by the diameter of the adjacent pulmonary artery, generally averages 0.65 to 0.70.[56] The presence of a bronchoarterial ratio of more than 1 in normal subjects has been associated with increased age.[56] The measurement has been found to be influenced by altitude, presumably as a result of the combination of hypoxic vasoconstriction and bronchodilatation. In one investigation of 17 normal, nonsmoking individuals living at 1600 m and 16 individuals living at sea level, the mean bronchoarterial ratio was 0.76 at altitude and 0.62 at sea level.[57] The bronchoarterial ratio may also appear to be more than 1 if the scan traverses an undivided bronchus near its branch point and its accompanying artery already has branched.[58]

Anatomically, the walls of large bronchi, outlined by lung on one side and air in the bronchial lumen on the other, appear smooth and of uniform thickness. The normal thickness of an airway wall is related to its diameter, with a normal bronchial wall thickness corresponding to approximately 10% to 30% of the bronchial diameter. Lobar to segmental bronchi (second to fourth generation) have a wall thickness of approximately 1.5 mm and a mean diameter between 5 and 8 mm. Subsegmental (sixth to eighth generation) bronchi have a wall thickness of approximately 0.3 mm and mean diameters between 1.5 and 3 mm. Currently, subsegmental bronchi are routinely identifiable; more distal airways (eleventh to thirteenth generation) have a wall thickness of 0.1 to 0.15 mm and diameters that measure 0.7 to 1 mm.[59] The visibility of normal bronchioles depends on their wall thickness rather than diameter. The smallest airways normally visible using HRCT have a diameter of approximately 2 mm and a wall thickness of 0.2 to 0.3 mm. The value

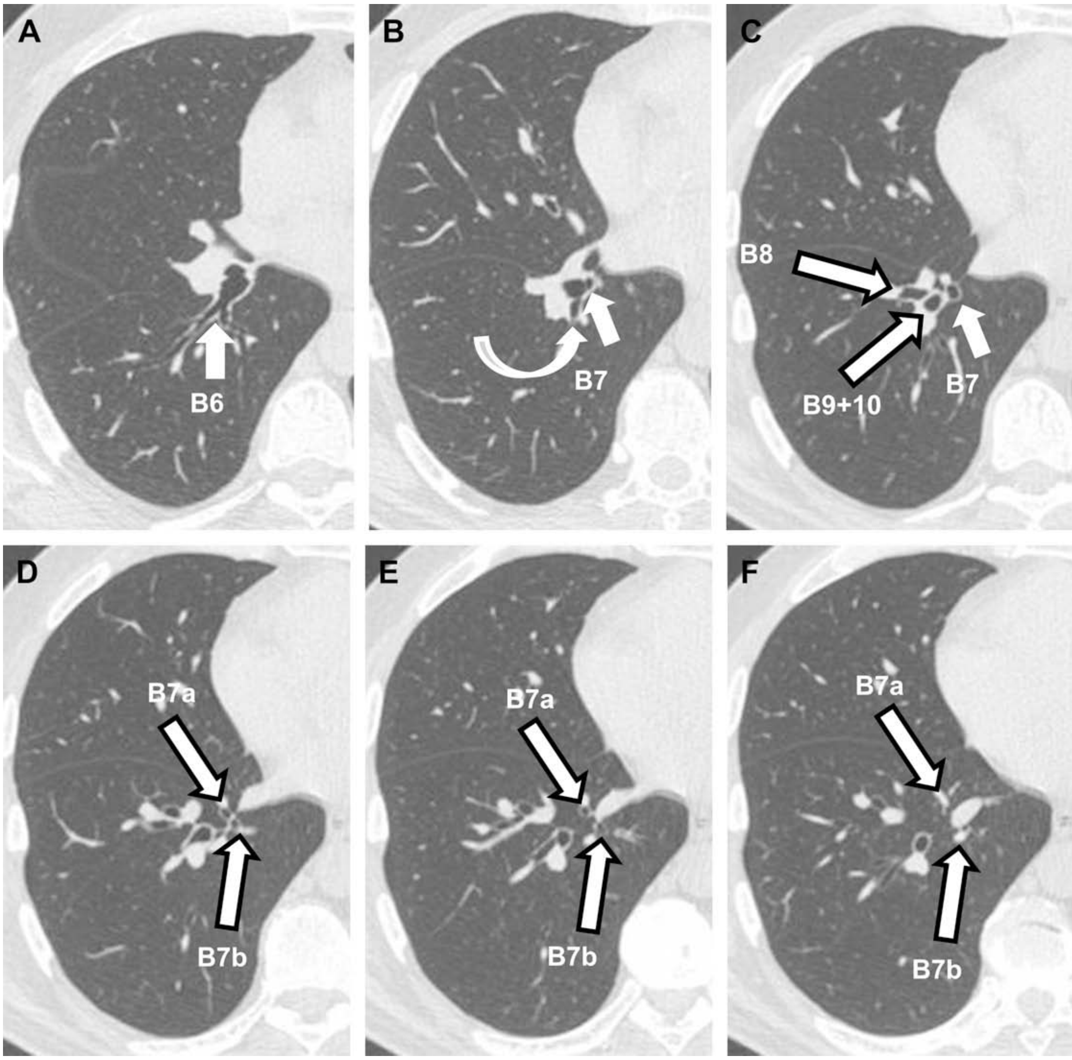

Fig. 10. Anatomic variations of the right bronchial tree. (*A–C*) Subsuperior segmental bronchus B*, accessory superior segmental bronchus or subapical bronchus, is a common variation of the right lower lobe originating below B6 (*A*) at a variable level from the truncus basalis down to the posterior segmental basilar bronchus. In this case, the origin is well seen in (*B*) at the posterior part of the B8 + 9 + 10 trunk (*curved arrow*), B7 lying medially. Successive origin of B8 and B9 + 10 in (*C*). (*D–F*) Most common variation of the subdivision of medial basilar segmental bronchus B7. In this case, the medial ramus B7b courses posterior to the inferior pulmonary vein, unlike the anterior ramus B7a, which remains anterior to the vein.

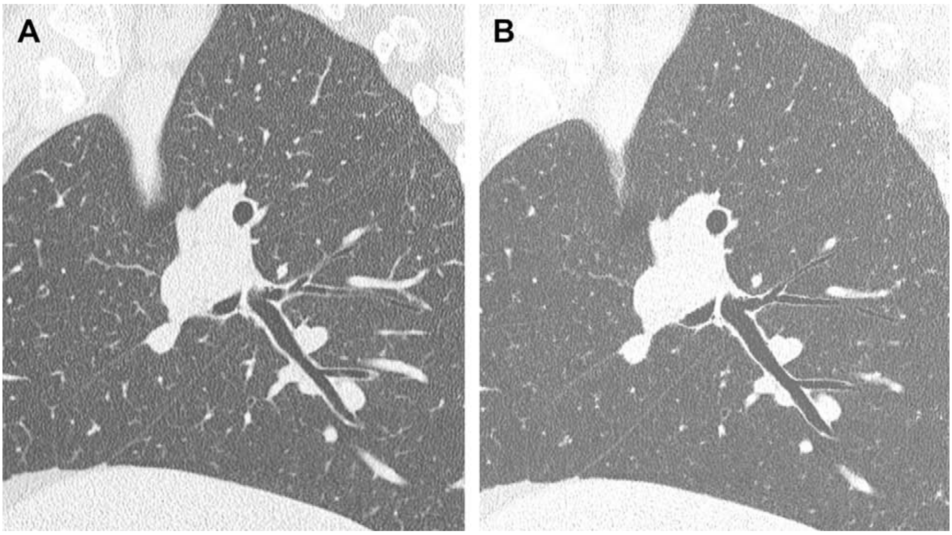

Fig. 11. (*A, B*) Subapical bronchus originates from the posterior basilar segmental bronchus of the right lower lobe. Single reformat (*left*) and thin mIP (*right*) allow visualization of the complete course of B6 and the abnormal bronchi, which have a similar horizontally posterior course.

of the caliber of a bronchiole supplying a secondary lobule, a terminal bronchiole, and a distal respiratory bronchiole is 1 mm, approximately 0.6 mm, and approximately 0.4 mm, respectively, and the thickness of its wall measures approximately 0.15 mm, 0.1 mm, and less than 0.1 mm, respectively.[58] As a result, normal bronchioles are not visible on CT scans. Airways are rarely seen within 1 cm of the pleural surface in most locations, except adjacent to the mediastinum.[57]

CT measurement slightly overestimates wall thickness because it also includes the surrounding peribronchial interstitium. The apparent bronchial wall thickness and diameter of bronchi are markedly influenced by the display parameters. The window and width levels that provide the most accurate measurement of bronchial caliber and wall thickness are −450 to −500 HU and 1000 to 1500 HU, respectively.[29,35,60] When an incorrect parameter is used, the error in estimating the thickness or size of a structure is related to its actual thickness or size, greater fractional overestimates, or underestimates being made for small structures.

In their study, Matsuoka and colleagues[56] found variation of airway caliber and wall area percentage within individual bronchi on cross-sectional CT sections in asymptomatic subjects without cardiopulmonary disease. In 32.7% of the sites observed in contiguous CT sections, the airway lumen did not decrease on the peripheral side, as classically expected. According to the authors, the proportions of epithelium, smooth muscle, interstitial connective tissue, and cartilage varying at different levels of the bronchus, variation within individual airway lumens, and wall area percentage may be based on variation of bronchial morphology. Quantitative evaluation of the degree of heterogeneous constrictor responses to bronchial challenge should include consideration of normal variation of airway lumen.

Expiratory HRCT may demonstrate lobular areas of air trapping in as many as 60% of normal patients. The prevalence of air trapping increases with age.[61-63] The dependent lung, the lung bases, and the superior segments of the lower lobes are most often concerned. The degree of air trapping that may be identified in normal patients remains controversial, however.

SUMMARY

The new generation of MDCT has revolutionized noninvasive imaging of proximal and distal airways. Exquisite anatomic details of the airway lumen and airway wall on axial CT images benefit in routine practice from postprocessing tools in adequate orientation, ensuring excellent assessment of the morphology and location of any pathologic condition. This technique may be combined with use of low-dose CT. The next challenge for CT is the functional assessment with accurate quantification of caliber and thickness of the whole bronchial tree integrated in the more complex evaluation of the lung parenchyma, including hypoattenuated areas.

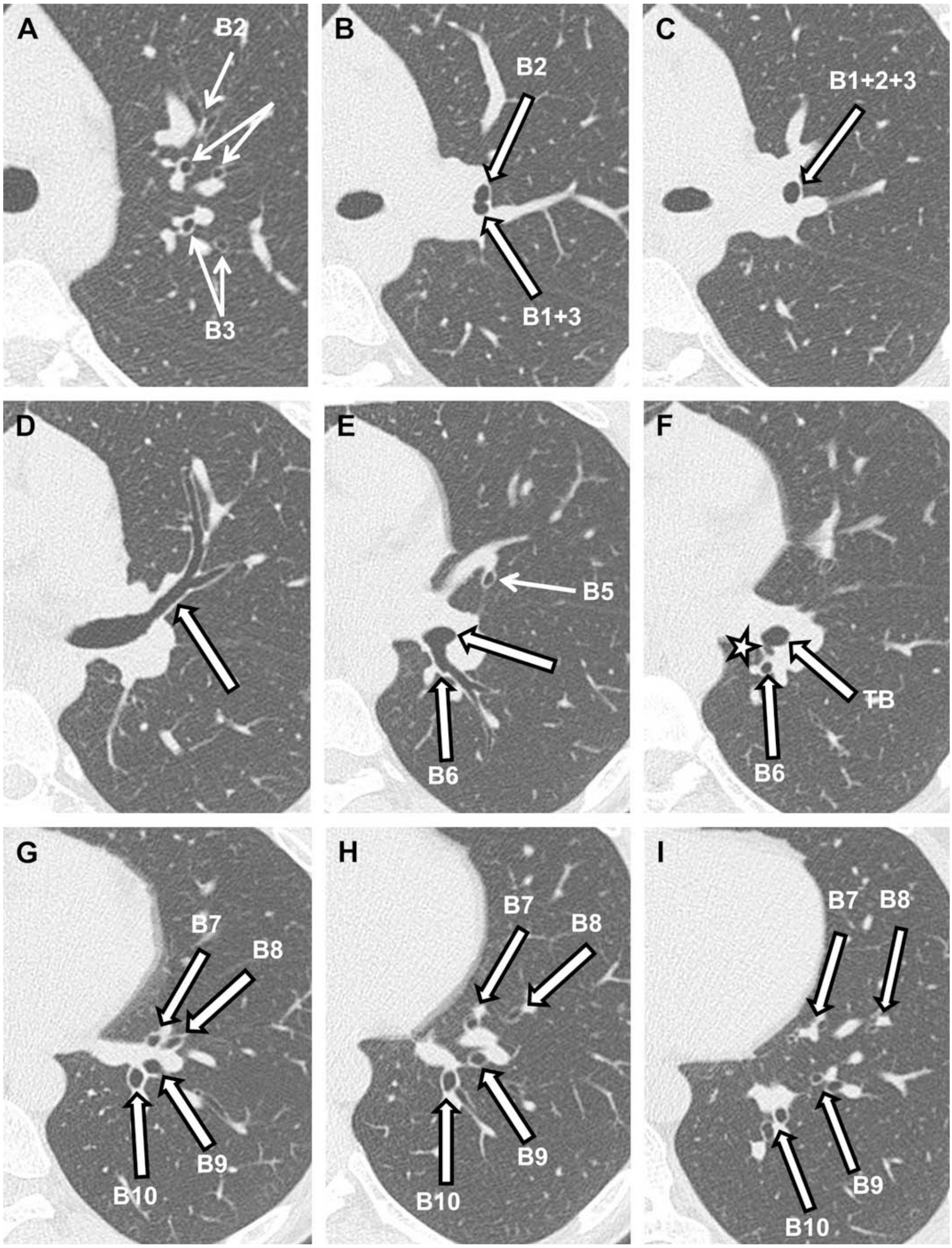

Fig. 12. Normal anatomy of the bronchi on the left side. The first Boyden's classification is used with successive 1-mm slices. (*A–C*) The left upper lobe bronchus bifurcates in most cases in an upper culminal bronchus (CB), which almost immediately divides into an apicoposterior (B1 + 3) and anterior (B2) segmental bronchus and in a lower division, the lingular bronchus. (*A*) Subsegmental divisions of B1, B2, B3 are shown (*arrows*). (*D–F*) The lingular bronchus (*arrow* in *D*) arises from the lower part of the left upper lobar bronchus (LULB), extends anteriorly and inferiorly for 2 to 3 cm, and then bifurcates into the superior (B4) and inferior divisions (B5). The course of B4 tends to be more lateral and horizontal than B5. Left lower lobar bronchus (LLLB) and B6 are similar to those on the right side. (*F*) Note that the rounded lucency corresponds to the medial subsegmental branch of B6 and that the lucency at the posterior part of the TB (*star*) corresponds to a subapical branch of the LLLB, more rarely seen on the left side than on the right side. (*G–I*) The truncus basalis is longer than on the right side and divides into three basal segmental bronchi, including anteromedial (B7 + 8), lateral (B9), and posterior (B10). (*J*) 3D volume rendering.

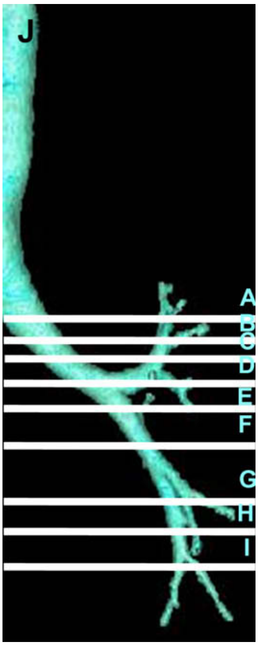

Fig. 12. (*continued*).

REFERENCES

1. Beigelman-Aubry C, Hill C, Guibal A, et al. Multidetector row CT and postprocessing techniques in the assessment of diffuse lung disease. Radiographics 2005;25:1639–52.
2. Grenier PA, Beigelman-Aubry C, Fetita C, et al. New frontiers in CT imaging of airway disease. Eur Radiol 2002;12:1022–44.
3. LoCicero J 3rd, Costello P, Campos CT, et al. Spiral CT with multiplanar and three-dimensional reconstructions accurately predicts tracheobronchial pathology. Ann Thorac Surg 1996;62:811–7.
4. Remy-Jardin M, Remy J, Deschildre F, et al. Obstructive lesions of the central airways: evaluation by using spiral CT with multiplanar and three-dimensional reformations. Eur Radiol 1996;6:807–16.
5. Beigelman-Aubry C. Post-processing and display in multislice CT of the chest. JBR-BTR 2007;90:85–8.
6. Arakawa H, Sasaka K, Lu WM, et al. Comparison of axial high-resolution CT and thin-section multiplanar reformation (MPR) for diagnosis of diseases of the pulmonary parenchyma: preliminary study in 49 patients. J Thorac Imaging 2004;19:24–31.
7. Remy J, Remy-Jardin M, Artaud D, et al. Multiplanar and three-dimensional reconstruction techniques in CT: impact on chest diseases. Eur Radiol 1998;8:335–51.
8. Salvolini L, Bichi Secchi E, Costarelli L, et al. Clinical applications of 2D and 3D CT imaging of the airways: a review. Eur J Radiol 2000;34:9–25.
9. Fraser RS, Muller NL, Colman N, et al. The normal lung: computed tomography. In: Fraser RS, Muller NL, Colman N, et al, editors. Diagnosis of diseases of the chest. 4th edition. Philadelphia: WB Saunders; 1999. p. 281–95.
10. Bhalla M, Naidich DP, McGuinness G, et al. Diffuse lung disease: assessment with helical CT. Preliminary observations of the role of maximum and minimum intensity projection images. Radiology 1996;200:341–7.
11. Remy-Jardin M, Remy J, Artaud D, et al. Diffuse infiltrative lung disease: clinical value of sliding-thin-slab maximum intensity projection CT scans in the detection of mild micronodular patterns. Radiology 1996;200:333–9.
12. Gruden JF, Ouanounou S, Tigges S, et al. Incremental benefit of maximum-intensity-projection images on observer detection of small pulmonary nodules revealed by multidetector CT. AJR Am J Roentgenol 2002;179:149–57.
13. Boiselle PM, Lynch DA. Anatomical airway imaging methods. In: Boiselle PM, Lynch DA, editors. CT of the airways. Totowa (NJ): Humana Press; 2008. p. 75–94.
14. Remy-Jardin M, Remy J, Artaud D, et al. Volume rendering of the tracheobronchial tree: clinical evaluation of bronchographic images. Radiology 1998;208:761–70.
15. Kauczor HU, Hofmann D, Kreitner KF, et al. Normal and abnormal pulmonary ventilation: visualization at hyperpolarized He-3 MR imaging. Radiology 1996;201:564–8.
16. Fetita C, Preteux F, Beigelman-Aubry C, et al. 3D bronchoview: a new software package for investigating airway diseases. [abstract]. Eur Radiol 2002;12:394.
17. Hopper KD, Iyriboz TA, Mahraj RP, et al. CT bronchoscopy: optimization of imaging parameters. Radiology 1998;209:872–7.
18. Boiselle PM, Reynolds KF, Ernst A. Multiplanar and three-dimensional imaging of the central airways with multidetector CT. AJR Am J Roentgenol 2002;179:301–8.
19. Summers RM, Selbie WS, Malley JD, et al. Polypoid lesions of airways: early experience with computer-assisted detection by using virtual bronchoscopy and surface curvature. Radiology 1998;208:331–7.
20. Newmark GM, Conces DJ Jr, Kopecky KK. Spiral CT evaluation of the trachea and bronchi. J Comput Assist Tomogr 1994;18:552–4.
21. Ferretti GR, Bricault I, Coulomb M. Virtual tools for imaging of the thorax. Eur Respir J 2001;18:381–92.
22. Newman KB, Lynch DA, Newman LS, et al. Quantitative computed tomography detects air trapping due to asthma. Chest 1994;106:105–9.

23. Zhang J, Hasegawa I, Hatabu H, et al. Frequency and severity of air trapping at dynamic expiratory CT in patients with tracheobronchomalacia. AJR Am J Roentgenol 2004;182:81–5.
24. Wittram C, Batt J, Rappaport DC, et al. Inspiratory and expiratory helical CT of normal adults: comparison of thin section scans and minimum intensity projection images. J Thorac Imaging 2002;17:47–52.
25. Nishino M, Hatabu H. Volumetric expiratory HRCT imaging with MSCT. J Thorac Imaging 2005;20: 176–85.
26. Fetita CI, Preteux F, Beigelman-Aubry C, et al. Pulmonary airways: 3-D reconstruction from multislice CT and clinical investigation. IEEE Trans Med Imaging 2004;23:1353–64.
27. Amirav I, Kramer SS, Grunstein MM, et al. Assessment of methacholine-induced airway constriction by ultrafast high-resolution computed tomography. J Appl Phys 1993;75:2239–50.
28. King GG, Muller NL, Whittall KP, et al. An analysis algorithm for measuring airway lumen and wall areas from high-resolution computed tomographic data. Am J Respir Crit Care Med 2000;161:574–80.
29. McNamara AE, Muller NL, Okazawa M, et al. Airway narrowing in excised canine lungs measured by high-resolution computed tomography. J Appl Phys 1992;73:307–16.
30. Perot V, Desberat P, Berger P, et al. Nouvel algorithme d'extraction des paramètres géométriques des bronches en TDMHR. [abstract]. J Radiol 2001;82:1213 [in French].
31. Prêteux F, Fetita CI, Capderou A, et al. Modeling, segmentation, and caliber estimation of bronchi in high resolution computerized tomography. J Electron Imaging 1999;8:36–45.
32. Wood SA, Zerhouni EA, Hoford JD, et al. Measurement of three-dimensional lung tree structures by using computed tomography. J Appl Phys 1995; 79:1687–97.
33. Okazawa M, Muller N, McNamara AE, et al. Human airway narrowing measured using high resolution computed tomography. Am J Respir Crit Care Med 1996;154:1557–62.
34. Seneterre E, Paganin F, Bruel JM, et al. Measurement of the internal size of bronchi using high resolution computed tomography (HRCT). Eur Respir J 1994;7:596–600.
35. Webb WR, Gamsu G, Wall SD, et al. CT of a bronchial phantom: factors affecting appearance and size measurements. Invest Radiol 1984;19:394–8.
36. Beigelman-Aubry C, Capderou A, Grenier PA, et al. Mild intermittent asthma: CT assessment of bronchial cross-sectional area and lung attenuation at controlled lung volume. Radiology 2002;223:181–7.
37. Brown R, Mitzner W, Bulut Y, et al. Effect of lung inflation in vivo on airways with smooth-muscle tone or edema. J Appl Phys 1997;82(2):491–9.
38. Brown RH, Georgakopoulos J, Mitzner W. Individual canine airways responsiveness to aerosol histamine and methacholine in vivo. Am J Respir Crit Care Med 1998;157:491–7.
39. King GG, Muller NL, Pare PD. Evaluation of airways in obstructive pulmonary disease using high-resolution computed tomography. Am J Respir Crit Care Med 1999;159:992–1004.
40. Nakano Y, Muro S, Sakai H, et al. Computed tomographic measurements of airway dimensions and emphysema in smokers: correlation with lung function. Am J Respir Crit Care Med 2000;162:1102–8.
41. Niimi A, Matsumoto H, Amitani R, et al. Airway wall thickness in asthma assessed by computed tomography: relation to clinical indices. Am J Respir Crit Care Med 2000;162:1518–23.
42. Gamsu G, Webb WR. Computed tomography of the trachea: normal and abnormal. AJR Am J Roentgenol 1982;139:321–6.
43. Holbert JM, Strollo DC. Imaging of the normal trachea. J Thorac Imaging 1995;10:171–9.
44. Boiselle PM, Ernst A. Tracheal morphology in patients with tracheomalacia: prevalence of inspiratory lunate and expiratory "frown" shapes. J Thorac Imaging 2006;21:190–6.
45. Naidich D, Webb WR, Grenier PA, et al. Introduction to imaging methodology and airway anatomy. In: Naidich D, Webb WR, Grenier PA, Harkin TJ, Gefter WB, editors. Imaging of the airways: functional and radiologic correlations. Philadelphia: Lippincott Williams & Wilkins; 2005. p. 1–28.
46. Boiselle PM, Lynch DA. Radiologic anatomy of the airways. In: Boiselle PM, Lynch DA, editors. CT of the airways. Totowa (NJ): Humana Press; 2008. p. 25–48.
47. Vock P, Spiegel T, Fram EK, et al. CT assessment of the adult intrathoracic cross section of the trachea. J Comput Assist Tomogr 1984;8:1076–82.
48. Breatnach E, Abbott GC, Fraser RG. Dimensions of the normal human trachea. AJR Am J Roentgenol 1984;142:903–6.
49. Woodring JH, Howard RS 2nd, Rehm SR. Congenital tracheobronchomegaly (Mounier-Kuhn syndrome): a report of 10 cases and review of the literature. J Thorac Imaging 1991;6:1–10.
50. Webb EM, Elicker BM, Webb WR. Using CT to diagnose nonneoplastic tracheal abnormalities: appearance of the tracheal wall. AJR Am J Roentgenol 2000;174:1315–21.
51. Olivier P, Hayon-Sonsino D, Convard JP, et al. Measurement of left mainstem bronchus using multiplane CT reconstructions and relationship between patient characteristics or tracheal diameters and left bronchial diameters. Chest 2006;130: 101–7.
52. Thurlbeck WM, Churg AM. Pathology of the lung. New York: Thieme Medical Publishers; 1995.

53. Boyden EA. The nomenclature of the bronchopulmonary segments and their blood supply. Dis Chest 1961;39:1–6.
54. Jackson CI, Huber JF. Correlated applied anatomy of the bronchial tree and lungs with a system of nomenclature. Dis Chest 1943;9:319–26.
55. Hayward J, Reid ML. The cartilage of the intrapulmonary bronchi in normal lungs, in bronchiectasis, and in massive collapse. Thorax 1952;7: 98–110.
56. Matsuoka S, Kurihara Y, Nakajima Y, et al. Serial change in airway lumen and wall thickness at thin-section CT in asymptomatic subjects. Radiology 2005;234:595–603.
57. Kim JS, Muller NL, Park CS, et al. Bronchoarterial ratio on thin section CT: comparison between high altitude and sea level. J Comput Assist Tomogr 1997;21:306–11.
58. Webb WR, Müller NL, Naidich DP. Normal lung anatomy. In: High-resolution CT of the lung. 3rd edition. Philadelphia: Lippincott Wiliams & Wilkins; 2009. p. 42–64.
59. Weibel ER. High resolution computed tomography of the pulmonary parenchyma: anatomical background. Presented at the Fleiszchner Society Symposium on Chest Disease. Scottsdale, AZ, April 21, 1990.
60. Bankier AA, Fleischmann D, Mallek R, et al. Bronchial wall thickness: appropriate window settings for thin-section CT and radiologic-anatomic correlation. Radiology 1996;199:831–6.
61. Mastora I, Remy-Jardin M, Sobaszek A, et al. Thin-section CT finding in 250 volunteers: assessment of the relationship of CT findings with smoking history and pulmonary function test results. Radiology 2001;218:695–702.
62. Tanaka N, Matsumoto T, Miura G, et al. Air trapping at CT: high prevalence in asymptomatic subjects with normal pulmonary function. Radiology 2003; 227:776–85.
63. Lee KW, Chung SY, Yang I, et al. Correlation of aging and smoking with air trapping at thin-section CT of the lung in asymptomatic subjects. Radiology 2000;214:831–6.